14 Geographic Effects

In most of the previous chapters we assumed a flat, uniform bottom boundary, but in many parts of the world the ground is neither flat nor uniform. Geographic variations can modify the boundary-layer flow, and in some cases generate circulations in conjunction with diurnal heating cycles. We have already touched on a few such flows, such as the drainage winds at night within a stable boundary layer. In this chapter we examine both geographically-generated and geographically-modified flows.

Many of the examples will be based on highly simplified and idealized hill structures and surface features, in order to make the problem tractable. Nevertheless, the results can be qualitatively applied to more realistic scenarios.
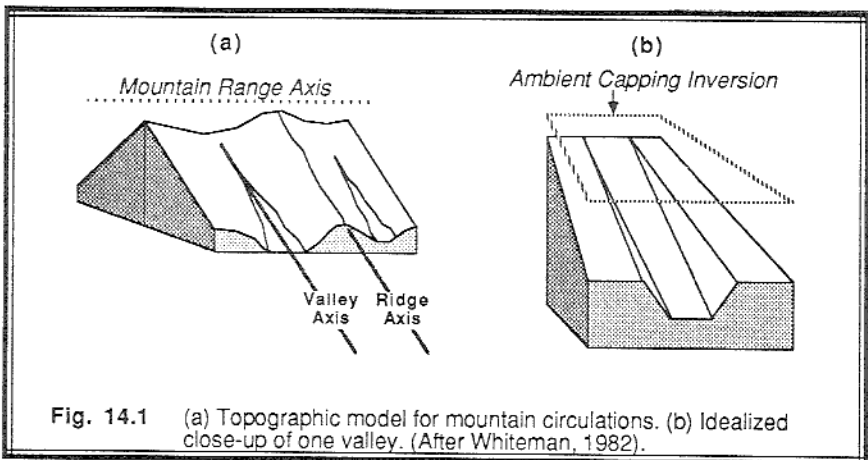
14.1 Geographically Generated Local Winds

Warming of mountain slopes by daytime sunlight or cooling by nocturnal radiation causes the air adjacent to the mountain to be warmed or cooled by conduction and turbulence. If the air near the mountain is at a different temperature than the ambient air at the same altitude over the center of the valley, then buoyant forces generate a circulation. Similar forcings occur over flat surfaces where albedo or heat capacity differences generate a horizontally inhomogeneous temperature field. In general, *local winds* are named after the source location of the wind: sea breezes come in from the sea, mountain winds come down from the mountain, etc.

In the following discussions we assume that the ambient winds are light or calm. For this situation the geographically-generated circulation can be studied without external influences. In many real situations, however, ambient synoptic or mesoscale winds can modify, or even eliminate the weak geographic circulations.

14.1.1   Circulations in Mountainous Regions

During the diurnal cycle in mountainous regions, three-dimensional circulations can form within and just above the valleys. We will initially examine the cross-valley-axis flow (anabatic/katabic *slope winds*) separately from the along-valley-axis flow (mountain/valley *valley winds*), and then combine the two components into a full three-dimensional picture (Geiger, 1965).

We will assume a topographic model as sketched in Fig 14.1 (Whiteman, 1982), with a river valley descending and deepening as it flows away from its source near the top of a mountain range. Along both sides of the valley and perpendicular to the mountain-range axis are ridges that also decrease in height. The valley is assumed to drain into a large open area such as a lake, ocean, plain, or a larger valley.

Fig. 14.1   (a) Topographic model for mountain circulations. (b) Idealized close-up of one valley. (After Whiteman, 1982).

Anabatic/Katabatic Cross-Valley Winds. We will start our diurnal cycle at sunset, where it is assumed that a deep daytime mixed layer extends well above the top of the mountain range, and that turbulence then decays to leave a neutrally stratified warm residual layer over the whole mountain and valley system (Fig 14.2a). Radiative cooling of the mountain surfaces cools the air adjacent to the surfaces, resulting in cold downslope or *katabatic winds*. These winds are very shallow (2 to 20 m), and have velocities on the order of 1 to 5 m/s. Above the valley floor, there is a gentle return circulation of upward moving air that diverges towards the ridges.

The chilled air flows into the valley and collects as a cold pool. Although some of the cold air flows down the valley axis, some can remain in the valley depending on the topography (Fig 14.2b). During the night, continued katabatic winds fill the cold air pool. Above the cold pool is the remaining warmer RL air, resulting in a temperature inversion capping the cold pool. The cold air from higher on the ridges flows downslope until it reaches an altitude where its temperature is the same as the temperature of the air in the valley. As a result, the coldest air sinks to the bottom of the pool, while the cooler air slides into the pool at higher altitudes (Fig 14.2c).
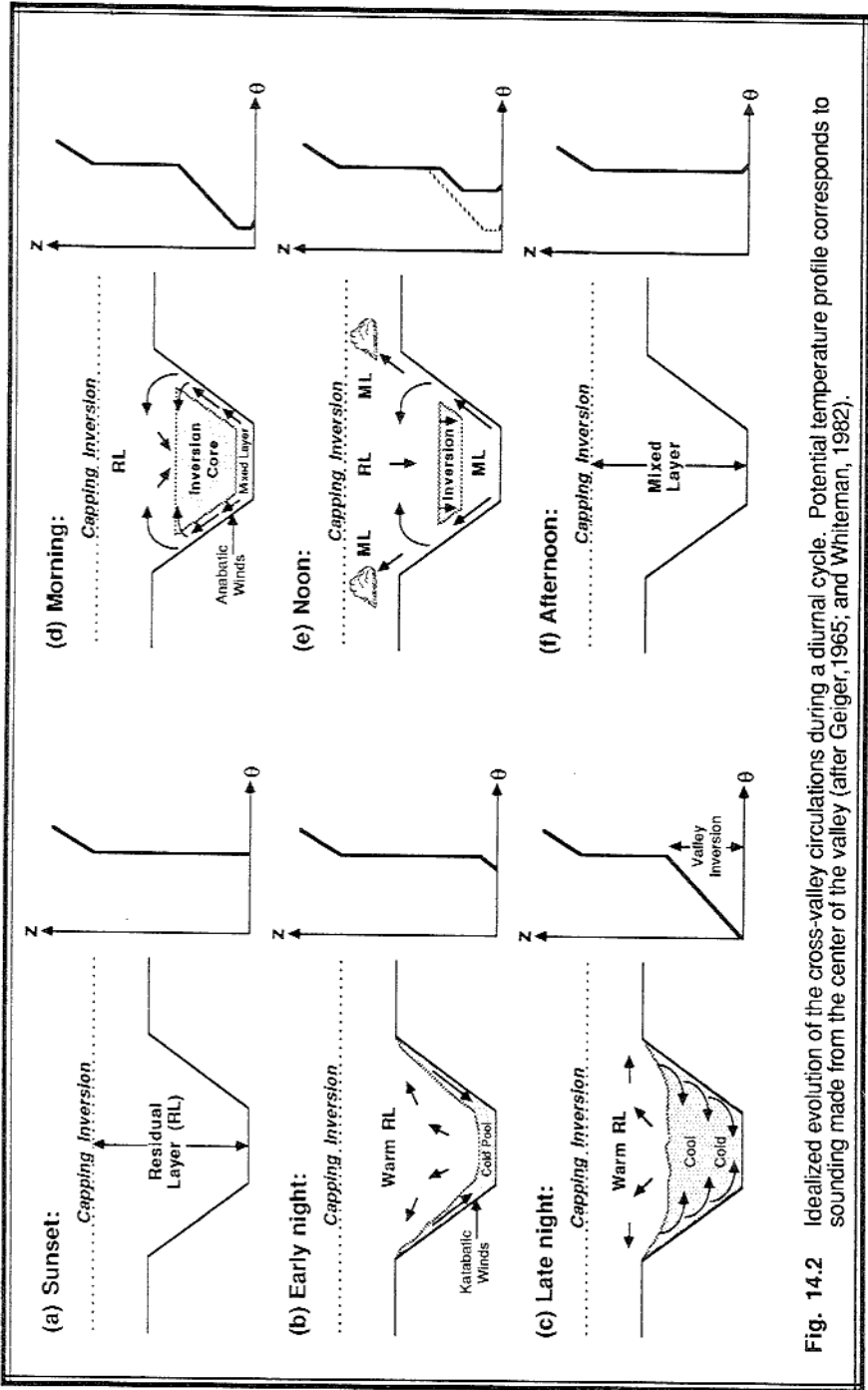
Fig. 14.2   Idealized evolution of the cross-valley circulations during a diurnal cycle. Potential temperature profile corresponds to sounding made from the center of the valley (after Geiger, 1965; and Whiteman, 1982).

The resulting pool is often stably stratified throughout its depth, and is sometimes called the *valley inversion*. Pollutants emitted into this inversion can build to high concentrations because of the trapping between the valley walls, and can be hazardous to people, animals, and plant life on the slopes.

After sunrise, solar heating warms the air near the valley walls, causing warm upslope *anabatic winds* (Fig 14.2d). These gentle winds (less than 1 m/s) tend to hug the valley walls as they rise, eventually breaking away at their level of neutral buoyancy, or at the top of the ridge. Sometimes cumulus clouds known as *anabatic clouds* form in the warm air rising along the ridge axes. Above the valley inversion there is gentle convergence and subsidence.

As this warmed air leaves the valley floor, the remaining pool of cold air sinks to replace it. In addition, solar heating of the valley floor itself causes a shallow mixed layer to form. Although this ML tends to grow by the entrainment processes discussed in Chapter 11, a portion of the ML air is continuously drained away by the anabatic winds, causing the ML to rise much more slowly than would otherwise be expected over flat terrain (Fig 14.2e). The balance between ML entrainment and valley-inversion subsidence varies from situation to situation, between the extremes of no ML growth to rapid growth with little subsidence (Whiteman, 1982). For the case sketched in Fig 14.2e, the top and bottom of the valley inversion evolve as shown in Fig 14.3.
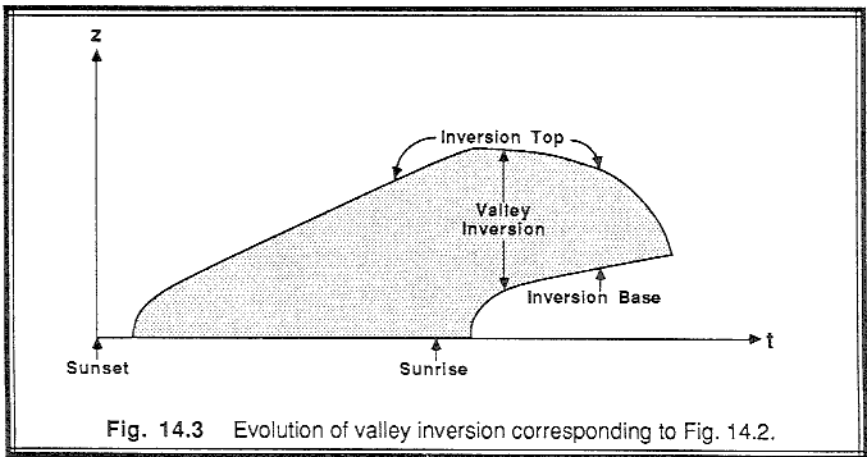

Fig. 14.3   Evolution of valley inversion corresponding to Fig. 14.2.

Eventually, the cold pool of air is completely eliminated, leaving a daytime convective mixed layer (Fig 14.2f). When this happens, the TKE can suddenly increase, sometimes to 6 times its earlier morning value (Banta, 1985). The diurnal cycle can then repeat itself.

In Figs 14.2d and e, the heating on both valley walls was idealized as being equal. In reality, the orientation of the valley walls relative to the sun position can cause one wall to be heated strongly, while the other is heated weakly or is in shadow. The resulting circulation is asymmetric, but otherwise proceeds as sketched.

Along-Valley Winds. At night, the cold winds flowing down the valley onto the plains are known as *mountain winds* or *drainage winds*. Depths range from 10 to 400 m, depending on the size and flow constrictions of the valley (Neff and King, 1987). Velocities of 1-8 m/s have been observed, and these winds are occasionally intermittent or surging. The return gentle circulation of warmer air aloft is called the *anti-mountain wind*, with velocities of about half of the mountain wind, and depths of about twice as much.

During the day, warm air gently flowing up the valley axis is known as the *valley wind*. This wind consists of a *valley-floor* component, and sometimes an *up-incline* component along the ridge tops. The cool, slow return flow aloft is called the *anti-valley wind*. Fig 14.4 shows these along-valley wind components.

Fig. 14.4 Along-valley winds: (a) daytime valley and anti-valley winds; and (b) nighttime mountain and anti-mountain winds.
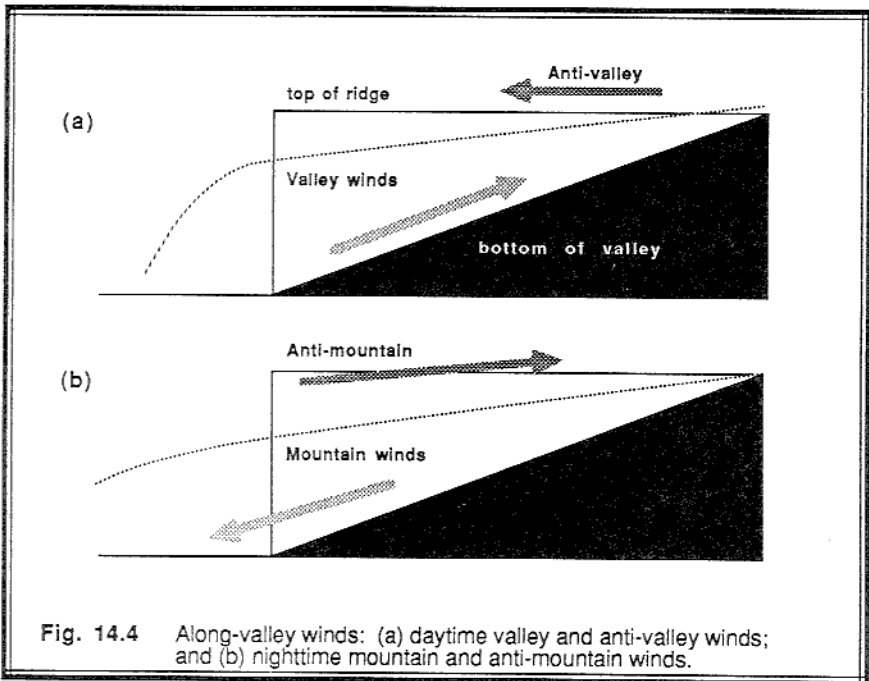
Three-dimensional Picture. At night, the 3-D circulation is fairly easy to picture, with downslope and down-valley winds converging just above the ground, and with gentle up-valley winds and divergence aloft (Fig 14.5a) (McNider and Pielke, 1984). During the morning, the picture is a bit more complicated, with the remaining elevated valley inversion continuing to slide down the valley as a stable core, riding above shallow up-valley and anabatic flows (Fig 14.5b, after Whiteman, 1982).

During the afternoon, after the stable core has disappeared, two counter-rotating helices are sometimes observed as the wind flows upslope and up-valley at low levels, and descends aloft over the center of the valley (Fig 14.5c).
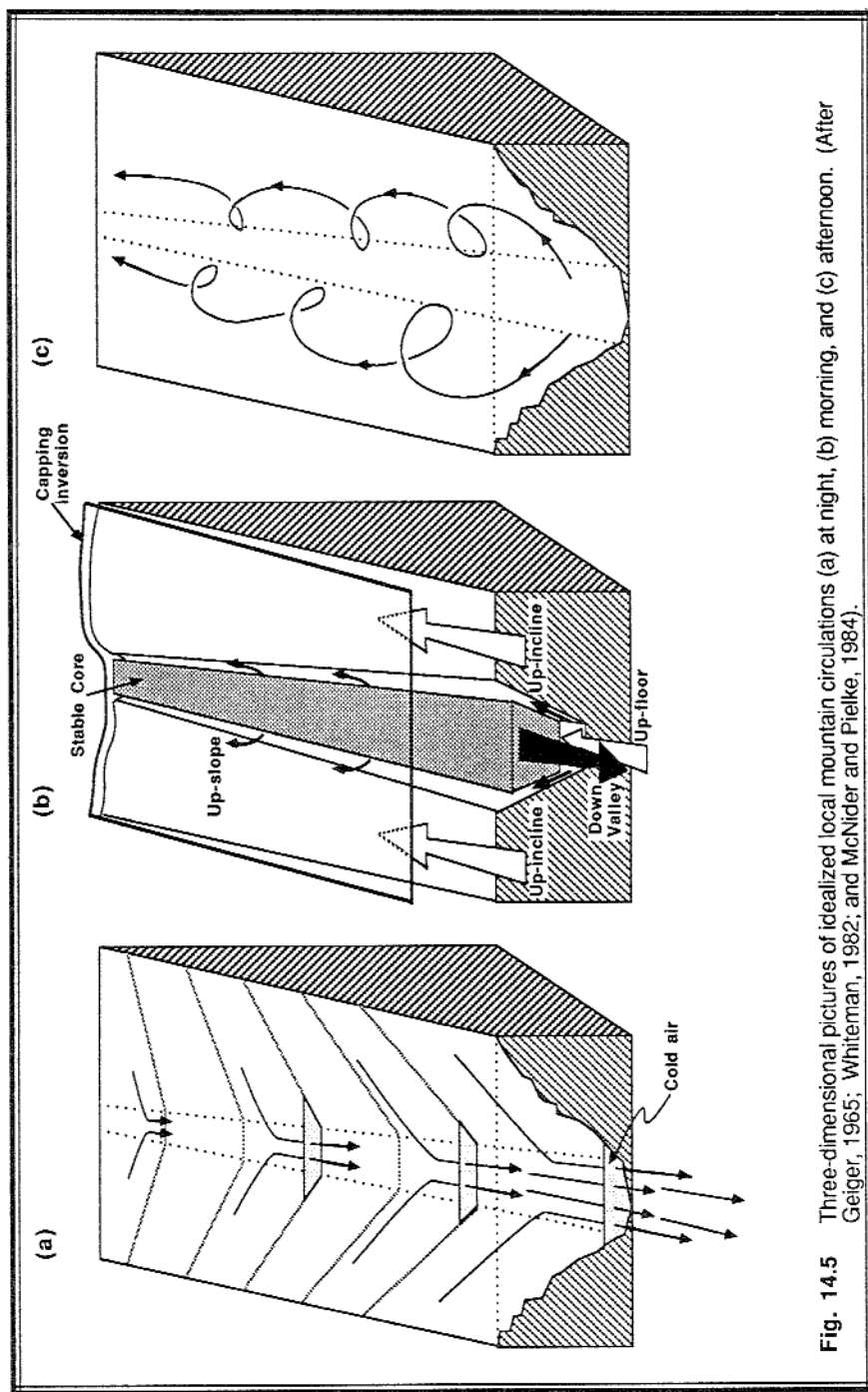
Fig. 14.5   Three-dimensional pictures of idealized local mountain circulations (a) at night, (b) morning, and (c) afternoon. (After Geiger, 1965; Whiteman, 1982; and McNider and Pielke, 1984).

14.1.2   Sea/Land and Inland Breezes

Sea and Lake Breezes. The large heat capacity of lakes and oceans reduces water-surface temperature change to near-zero values during a diurnal cycle. The land surface, however, warms and cools more dramatically because the small molecular conductivity and heat capacity in soils prevents the diurnal temperature signal from propagating rapidly away from the surface. As a result, the land is warmer than the water during the day, and cooler at night. This scenario is ideal for the formation of sea breezes (Lyons, 1975; Simpson, et al., 1977; Helmis, et al., 1987; Ogawa, et al., 1986).

During mid-morning (1000 local time) after the nocturnal SBL has been eliminated, air begins to rise over the warm land near the shoreline, and cooler air from the water flows in to replace it. This is known as the *sea-breeze* (or *lake breeze*). The inland limit of cool air progression over land is known as the *sea-breeze front*, and is marked by low-level convergence (in a band about 1 to 2 km wide), a marked temperature drop (often several °C; hence, it is a mesoscale cold front; see Fig 14.6), an increase in humidity, upward motion (of about 0.5 to 2.5 m/s), and sometimes enhanced cumulus clouds. A return circulation (the *anti-sea-breeze*) of 1 to 2 m/s aloft brings the warmer air back out to sea where it descends toward the sea surface to close the circulation (Fig 14.7). The depth of the sea breeze has been observed to be on the order of 100 to 500 m, and the total circulation depth including the return circulation can range from 500 m to 2000 m.
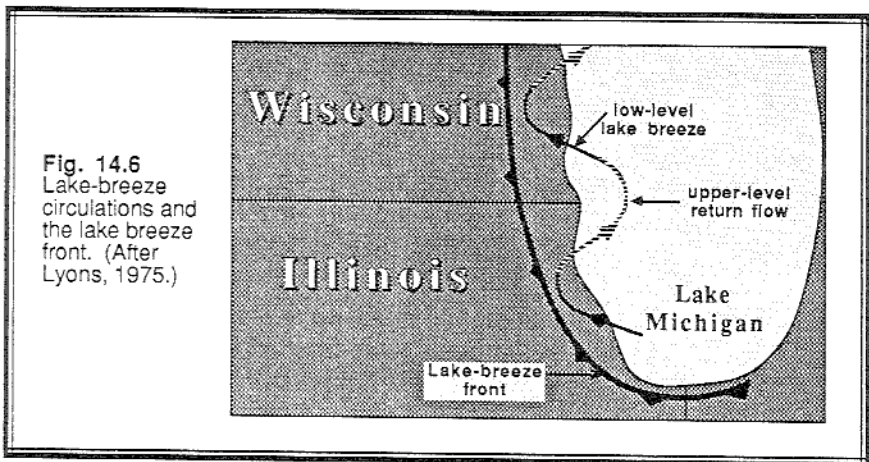

Fig. 14.6 Lake-breeze circulations and the lake breeze front. (After Lyons, 1975.)

In some cases the nose of the sea-breeze front can be about twice the depth of the trailing flow. The trailing flow is usually faster than the propagation rate of the front, with speeds of up to 5 to 7 m/s. As this flow approaches the surface front, a vortex-like pattern sometimes forms at the nose of the flow. After sea-breeze frontal passage the turbulence state of the cooler air quickly reaches a new local equilibrium, and scales to free convection similarity. The TKE intensity in the nose of the sea breeze can be on the order of twice that of the later equilibrium state (Briere, 1987).

In the absence of a background synoptic flow, the front progresses inland normal to the coastline at speeds of 1 to 5 m/s. It can easily reach 20 to 50 km inland by the end of the day. During the daytime, the sea-breeze front is driven partially by the active conversion of available potential energy to kinetic energy. After sunset, the front can continue to progress inland in the form of a gravity or density current similar to the thunderstorm gust front.
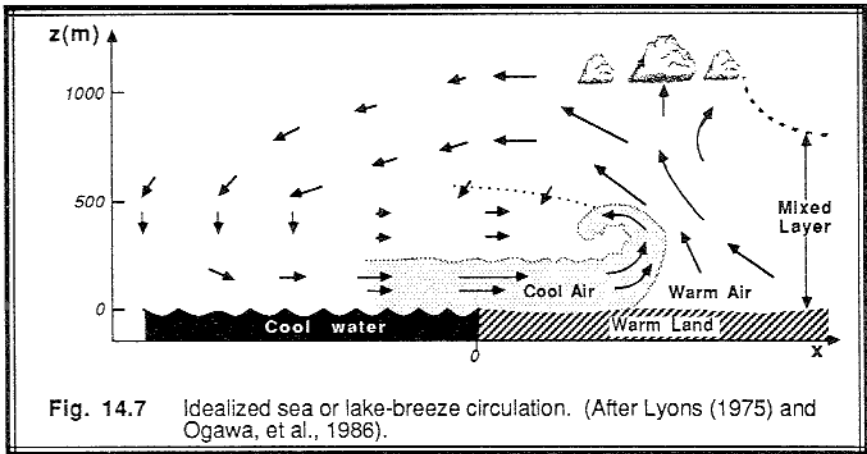

Fig. 14.7   Idealized sea or lake-breeze circulation. (After Lyons (1975) and Ogawa, et al., 1986).

Near capes and peninsulas, sea-breeze fronts from opposite shores converge and collide during the day, producing stronger upward motion. This phenomena is known to trigger thunderstorms in southern Florida (Pielke, 1974), and is believed to trigger cloud lines and possibly a bore wave in northern Australia (Noonan and Smith, 1986).

The sea-breeze wind direction at low-levels often turns under the influence of the Coriolis force and the baroclinicity between land and sea. For example, the winds along the western shore of Lake Michigan blow from east to west in the morning, and gradually rotate to blow from the southeast to northwest (Fig 14.6) by late afternoon (Lyons, 1975). Pollutants emitted into the sea breeze can thus be recirculated back further up the coastline.

If the background synoptic flow is in the same direction as the low-level sea-breeze and there are no major barriers to the flow, then the sea-breeze front can progress much further inland (over 100 km). It has been observed to flow over small mountain ranges such as the coastal range in Oregon (Mahrt, personal communication). Some fronts in England have taken over 10 h to reach 100 km inland (Simpson, et al, 1977). Garratt (1985) reported sea-breeze fronts occasionally reaching as far inland as 400 km in Australia. The speed of the front is well approximated by a linear sum of the imposed background wind component perpendicular to the front, and the speed of the front in still air (Pearson, et al., 1983).

During opposing synoptic flow, the sea-breeze can stall near the shoreline, or can be totally eliminated as the mean wind flows from land to sea. For synoptic flow parallel to the coastline, some observations indicate that the sea-breeze front becomes broader and

more diffuse. In many parts of the world we find mountains bordering the sea. At these locations both the sea breeze and the valley breeze can interact and unite to form stronger flows, or can counteract and oppose each other (Fitzjarrald, 1984, 1986; Kitada, 1986; Wakimoto and McElroy, 1986; Neff and King, 1987). The occasional presence of low-level jets near these mountainous coasts can also be superimposed on the mountain and sea breezes.

Sea-breeze circulations have been modeled both analytically (Rotunno, 1983) and numerically. The simpler models are often two-dimensional, hydrostatic, nonturbulent, steady-state approximations, where crosswind uniformity and sometimes linearity are assumed . Some of the more sophisticated models have used third-order closure or three dimensions (Martin and Pielke, 1983; Briere, 1987).

Land Breeze. At night, land surfaces usually cool faster than the neighboring water bodies, reversing the temperature gradient that was present during the day. The result is a *land breeze*: cold air from land flows out to sea at low levels, warms, rises, and returns aloft toward land (*anti-land-breeze*) where it eventually descends to close the circulation. The land breeze is believed to be analogous to the sea breeze, although there have been insufficient observations of its propagation across the water to be conclusive.

Inland Sea Breeze. Some modeling studies have suggested that mesoscale variations of surface moisture over land can induce mesoscale circulations analogous to the sea breeze (Segal and Pielke, 1987; Yan and Anthes, 1987, personal communication). This type of circulation, called the *inland sea breeze*, is believed to be strongest where moist vegetated surfaces are adjacent to drier surfaces. In some cases, the circulations in these regions might be large enough to trigger or enhance precipitation.

It is believed that swaths of moist soil from a previous thunderstorm passage over an otherwise dry land surface can create a sufficiently large moisture inhomogeneity to generate the inland sea breeze. In the western plains of the United States, large farms using center-pivot irrigation systems or banded irrigated crops can also create the necessary surface inhomogeneities. Deforestation and urbanization might be similar mechanisms causing inadvertent climate modification.

14.2   Geographically Modified Flow

When air flows over a variety of surfaces, each surface characteristic affects the flow. For example, suppose that there is a flat semi-infinite plot of land that is dry, unvegetated, and smooth. Downwind of that plot is another flat plot that is vegetated, moist, and rough. A boundary layer will develop over the first field that is in equilibrium with the surface forcings. When this air crosses the border and flows over the neighboring field, the bottom of the boundary layer will be modified by the new surface features, and the depth of this modified air will increase with distance downwind of the border. Above this modified layer, the boundary layer does not "feel" the new surface, and continues to behave as it did over the upwind surface.

14.2.1 The Internal Boundary Layer and Fetch

Definitions. The air that is modified by flow over a different surface is called an *internal boundary layer* (IBL), because it forms within an existing boundary layer. When surface heat flux changes across the border between two surfaces, the modified air is called a *thermal internal boundary layer* (TIBL) (Lyons, 1975; Garratt, 1987). For a change in roughness with no change in surface heat flux or stability, the generic name internal boundary layer is usually used.

The distance, x, downwind from a change in surface features is called *fetch*. When making surface-layer measurements, it is desirable to locate the instrument mast far enough downwind of the border so that the depth of the internal boundary layer, δ, is greater that the height of the mast (see Fig 14.8). Thus, with sufficiently large fetch, the surface-layer measurements are characteristic of the local field in which the instruments are located (Gash, 1986). For this reason, many surface-layer measurements are made within large uniform farm fields, meadows, pasture land, or forests.
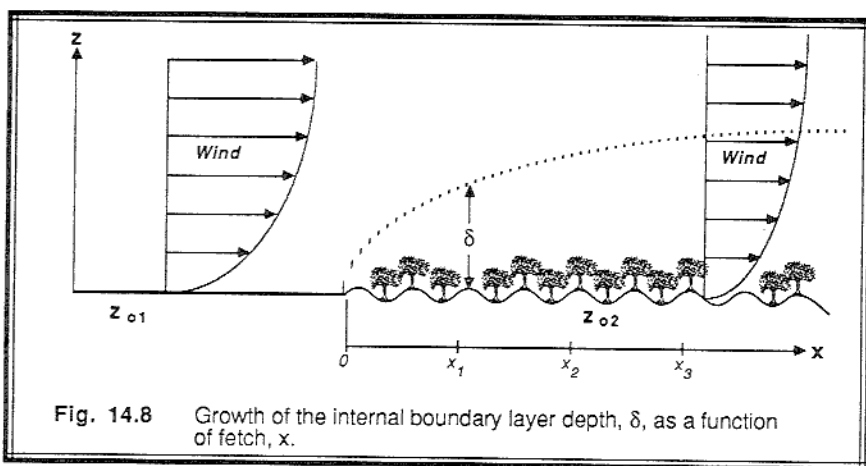

Fig. 14.8   Growth of the internal boundary layer depth, δ, as a function of fetch, x.

Change in Roughness. The IBL depth is often parameterized as a power of the fetch (Panofsky, et al., 1982; Smedman-Högström and Högström, 1978; Rao, et al., 1974):
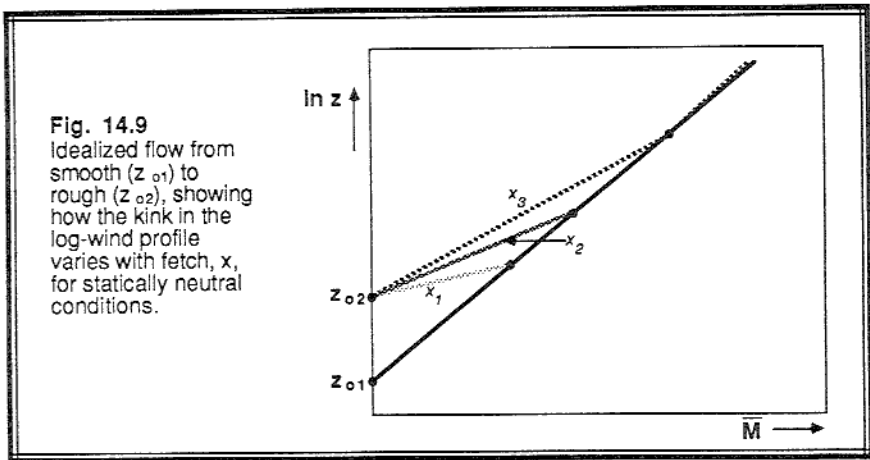
$$\frac{\delta}{z_{o1}} = a_{IBL} \cdot \left(\frac{x}{z_{o1}} \right)^{b_{IBL}} \qquad (14.2.1a)$$

where z_{o1} and z_{o2} are the aerodynamic roughness lengths upwind and downwind of the border. The power, b_{IBL}, is equal to about 0.8 for statically neutral conditions, but is slightly smaller (0.6 to 0.7) in statically stable conditions, and larger for unstable (0.8 to 1.0). Parameter a_{IBL} is in the range of 0.2 to 0.8, being large for unstable conditions

and small for stable ones. Sometimes, a_{IBL} is parameterized as a function of both roughnesses:
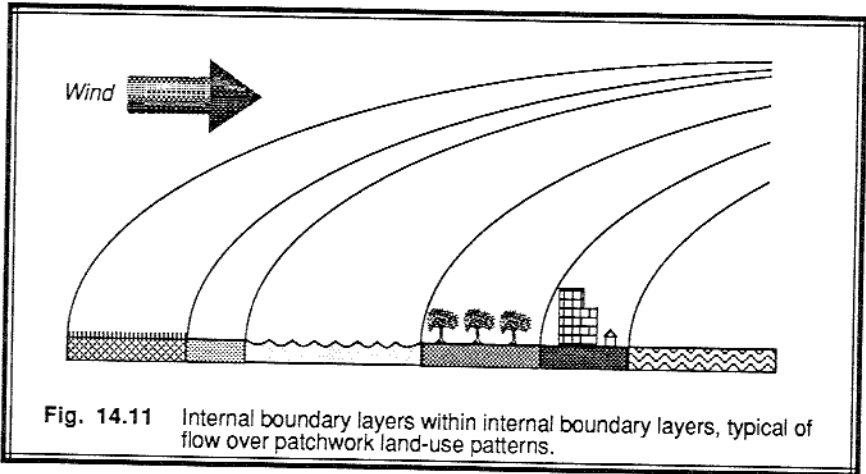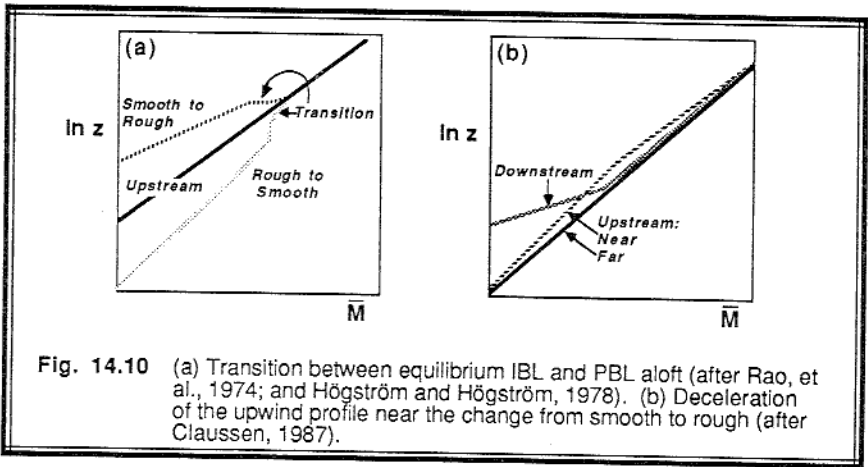
$$a_{IBL} = 0.75 + 0.03 \ln\left(\frac{z_{o2}}{z_{o1}} \right) \qquad (14.2.1b)$$

Fig 14.9 shows the idealized evolution of the statically-neutral logarithmic wind profile as a function of fetch, for the case of flow from a smooth to a rough surface. At fetch x_1 (see Fig 14.8) only a shallow layer "feels" the increased roughness. At greater distances, deeper layers feel the increased roughness. Above the top of the IBL (i.e., above the kink in the lines), the wind maintains a profile characteristic of the upwind roughness (Beljaars, 1987).

Fig. 14.9 Idealized flow from smooth (z_{o1}) to rough (z_{o2}), showing how the kink in the log-wind profile varies with fetch, x, for statically neutral conditions.

Smedman-Högström and Högström (1978) and Rao, et al. (1974) have shown that real wind profiles often exhibit a transition zone between the equilibrium IBL and the PBL aloft (Fig 14.10a). Also, Claussen (1987) suggests that the change in roughness can be felt a small distance ($x \cong 300\ z_o$) upstream of the boundary, resulting in a modification of the upwind profile (Fig 14.10b). Flow near the ground is slightly reduced for a change from smooth to rough, and flow aloft accelerates slightly.

In many parts of the world, there is a patchwork of surface features such as towns, farms, forests, lakes, etc. As sketched in Fig 14.11, this leads to IBLs within IBLs, with many kinks in the log-wind profile (Oke, 1978). When we combine kinks due to IBLs with curvature of the wind profile in diabatic conditions and curvature associated with a nonzero displacement distance, we find a very complicated wind profile. When hills are also considered, the result is complex indeed (Beljaars, et al., 1987).

Fig. 14.10 (a) Transition between equilibrium IBL and PBL aloft (after Rao, et al., 1974; and Högström and Högström, 1978). (b) Deceleration of the upwind profile near the change from smooth to rough (after Claussen, 1987).

Fig. 14.11 Internal boundary layers within internal boundary layers, typical of flow over patchwork land-use patterns.

When air flows from a smooth surface to a rough surface, the air in the IBL decelerates. This results in horizontal convergence and upward motion above the boundary between smooth and rough (Fig 14.12). Similarly, flow from rough to smooth causes divergence and subsidence. These vertical motions interact with other convective motions and affect pollutant transport. A convergence/divergence dipole is often observed at the upwind/downwind borders of cities, because of the change in roughness.

Upwind of a surface change from smooth to rough the friction velocity decreases slightly, then has a step increase overshooting its final equilibrium value, and finally decays to a final equilibrium state that is larger than the friction velocity over the smooth surface (Claussen, 1987). Turbulence kinetic energy also increases in a shallow layer at the point of roughness increase, then the layer of increased TKE grows in thickness as the IBL grows, and finally the surface value decreases to a new equilibrium value that is
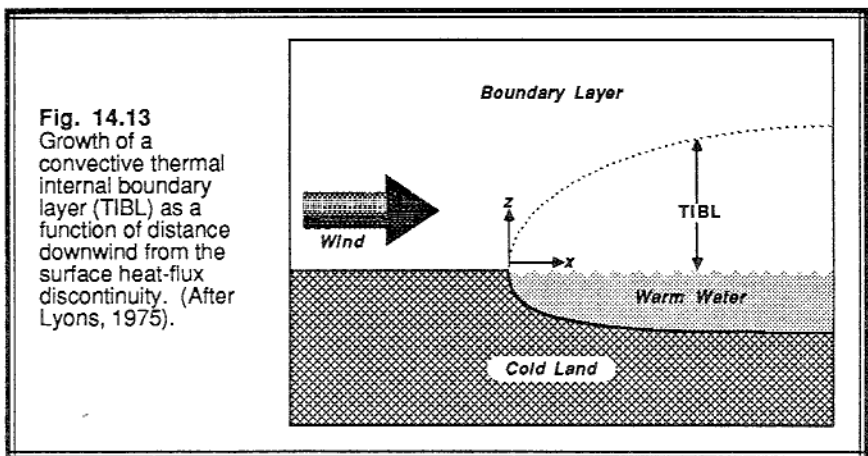
larger than the upwind surface value. Panofsky, et al. (1982) showed that most of the increase in TKE is associated with the smaller-size eddies in the spectrum.

Fig. 14.12   Isolines of [W / M $_{upwind}$] x 100 for flows over a roughness transition at $x/z_0 = 0$: where $z_{02}/z_{01} = 10^2$. (After Claussen, 1987).
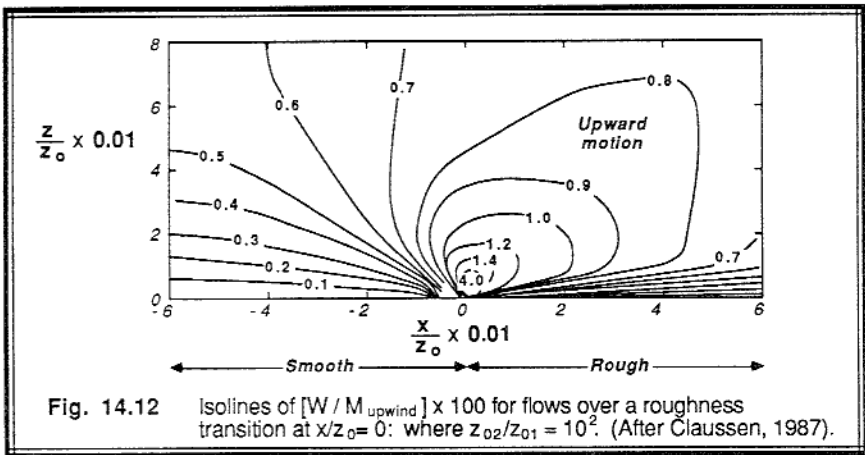
14.2.2 Thermal Internal Boundary Layer (TIBL)

Shorelines are good examples of regions where surface heat flux differences between neighboring surfaces can cause TIBLs. Although we will frequently use the word "shoreline" in this subsection, one should recognize that similar physics applies to other borders as well, such as between two land surfaces with differing albedoes and surface heat fluxes.

Convective TIBL. When air flows from a cooler to a warmer surface, a steady-state convective ML (*convective TIBL*, in this case) forms and deepens with distance downwind of the shoreline (Fig 14.13).   Turbulence is vigorous over the bulk of the

Fig. 14.13
Growth of a convective thermal internal boundary layer (TIBL) as a function of distance downwind from the surface heat-flux discontinuity. (After Lyons, 1975).

convective TIBL, and there is a relatively sharp, well-defined top. The ML depth, z_i, grows by entrainment, is suppressed by subsidence, and otherwise evolves as previously discussed for ML growth (Lyons, 1975; Venkatram, 1977; Hsu, 1986; Arritt, 1987; Hanna, 1987; Mitsuta, et al., 1986). TIBLs can occur in winter as cold continental air advects over warmer water, and in summer as air over colder water advects over warmer land.

Taylor's hypothesis can be invoked to transform the prognostic equations into gradient equations. Namely, apply (11.2.1b-e) to a column of air translating along with the mean wind. Pick a coordinate system with the x-axis perpendicular to the shoreline, and assume uniformity in the y direction. The result is:

$$\frac{\partial z_i}{\partial x} = \frac{w_e + w_L}{\overline{U}} \tag{14.2.2a}$$

$$\overline{U}\, z_i \frac{d<\overline{\theta}>}{dx} = \overline{w'\theta'}_s - \overline{w'\theta'}_{z_i} \tag{14.2.2b}$$

Similar equations can be written for moisture and winds.

Just as the ML can be shown to grow with the square root of time for special cases, the TIBL grows with the square root of distance from the shore. For example, Venkatram (1977) has suggested the following equation for TIBL depth as a function of distance, x:

$$z_i = \left[\frac{2\, C_D \left| \overline{\theta}_{land} - \overline{\theta}_{sea} \right| x}{\gamma\, (1 - 2\, A_R)} \right]^{1/2} \tag{14.2.2c}$$

where γ is the vertical potential-temperature gradient immediately above the TIBL, and A_R is an entrainment coefficient in the range of 0 to 0.22. Near shore, Hsu (1986) found for some cases that $z_i = 1.91 \cdot x^{1/2}$.

As the column of air advects downwind and warms, the temperature difference between the air and the ground lessens. As a result, the heat flux at the ground decreases, the mixed layer warms less rapidly, and the rise rate of the mixed layer is reduced. At large distances downwind of the shoreline, the air column is assumed to reach a state of equilibrium with (i.e., at the same temperature as) the underlying surface, with no surface heat fluxes and little or no entrainment. Mean variables approach this equilibrium state exponentially with distance, while heat fluxes approach zero exponentially.

An *air mass* is defined to be a boundary layer that has remained stationary over one location (the *source region*) long enough (days to weeks) to acquire some of the

characteristics of the underlying surface. When one air mass moves away from its source region over a surface of different temperature or moisture, the process is called *air mass modification*. The TIBL is just one type of air mass modification.

Stable TIBL. For flow from a warmer to a cooler surface, a *stable TIBL* forms analogous to the SBLs discussed in Chapter 12. Immediately downwind of the surface change one finds decaying residual turbulence that is very effective at mixing some of the cooler air upward. Further downwind, the static stability suppresses turbulence, except near the surface and near other shear zones where mechanical TKE production still occurs. For these well-developed stable TIBLs, turbulence decreases with height to a poorly defined top (just as in the nonadvective SBL).

Garratt (1987) suggests that the depth of the stable TIBL increases with the square-root of distance:

$$h = 0.014 \, \overline{M} \left[\frac{x \, \overline{\theta}}{g \, \overline{\Delta\theta}} \right]^{1/2} \tag{14.2.2d}$$

where $\Delta\theta$ is the initial temperature difference between the air (before growth of the TIBL) and the new cooler surface, and x is the distance from the surface change, measured in the direction of the mean wind. As the bottom of the stable TIBL cools and approaches the surface temperature, the above equation becomes invalid because the surface heat flux approaches zero. Beyond this point there is no further change in TIBL depth except for that caused by subsidence.

14.2.3 Flow Over Hills

Stable Stratification and the Froude Number. In statically stable conditions, perturbed air parcels oscillate vertically at the Brunt-Väisälä frequency, N_{BV}. When this oscillating air is imbedded in an air mass moving at mean wind speed $\overline{M}$, a wave is traced by the parcel. This oscillation has a wavelength proportional to $2\pi\overline{M}/N_{BV}$, which represents a natural wavelength of the air. If the length of the obstacle disturbing the flow is W_T, then we can write its effective wavelength as $2W_T$. The ratio of the natural wavelength of the air to the effective wavelength of the obstacle is defined as the internal *Froude number*:

$$Fr = \frac{\pi \, \overline{M}}{N_{BV} \, W_T} \tag{14.2.3a}$$

Frequently, this number is defined without the factor π. The Froude number is also sometimes described as the ratio of inertial to buoyant forces.

Fig. 14.14   Idealized flow over an isolated hill. The Froude number (Fr) compares the natural wavelength of the air to the width of the hill (W_H).
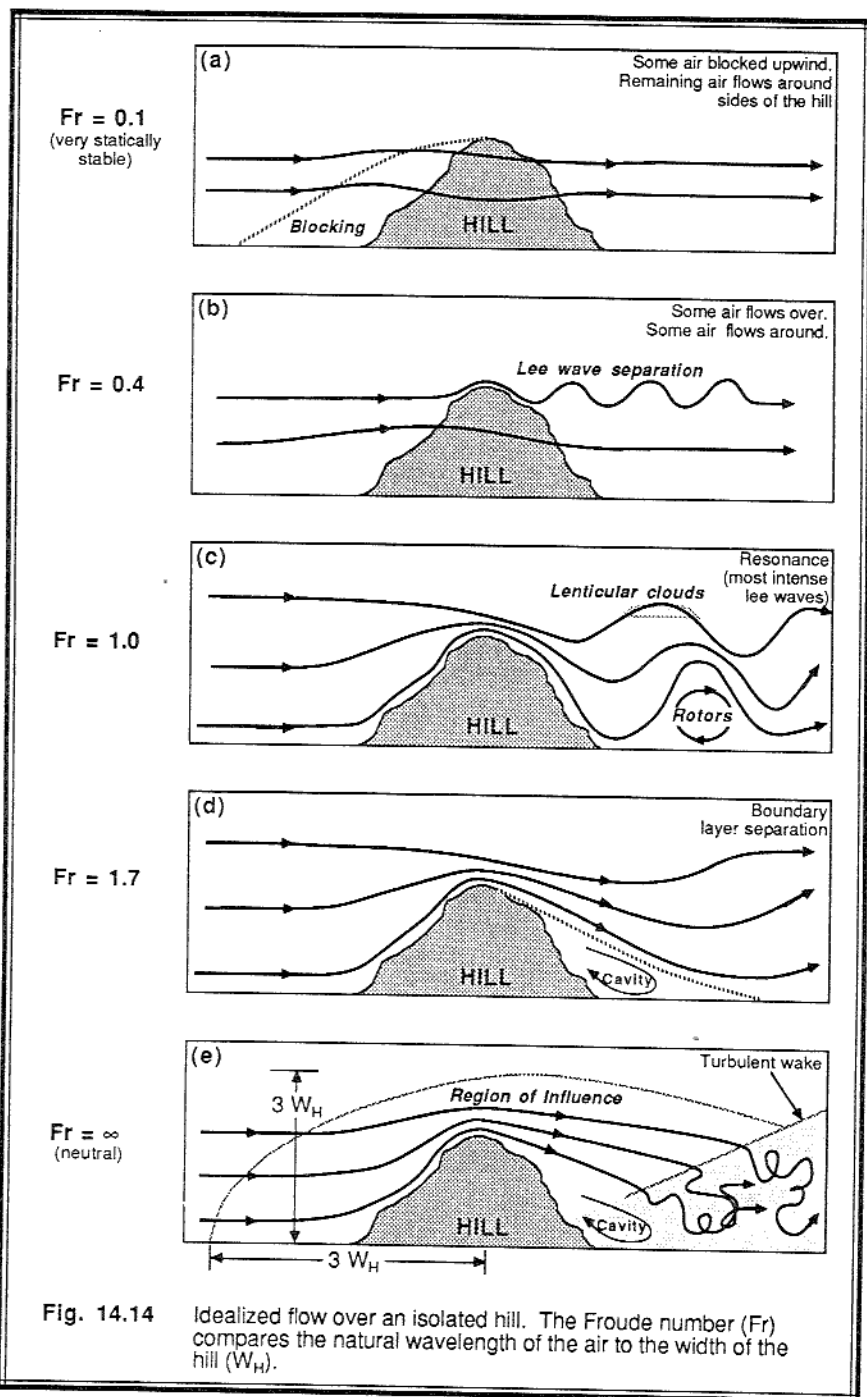
Fig 14.14 shows the variety of flows that are possible for different Froude numbers, for the special case of an isolated hill (Hunt, 1980). For strongly stable environments with light winds (i.e., Fr $\cong$ 0.1), air would rather flow around the hill than over it (Fig 14.14a). Directly upwind of the hill, some of the air is *blocked* by the hill and becomes stagnant. The combination of the blocked air and the hill acts like a larger, more streamlined obstacle, around which the remaining air must flow.

For slightly faster winds or weaker stability (i.e., Fr $\cong$ 0.4), some of the air flows over the top of the hill, while air at lower altitudes separates to flow around the hill (Fig 14.14b). Air that flows over the top has a natural wavelength much smaller than the size of the hill, and is perturbed by the hill to form lee waves. This *lee-wave separation* from the hill top is above the non-oscillating air that flows around the hill. For a column of air (air depth = hill height) approaching the center of the hill, the fraction of the column that flows over the top is approximately equal to Fr:

$$\frac{z_{LW}}{z_{hill}} = Fr \qquad\qquad (14.2.3b)$$

where z_{LW} is the depth of the column flowing over the hill that forms lee waves, and z_{hill} is the total depth of the column of air (equal to the height of the hill).

At a Froude number of 1.0, the stability is weaker and the winds are stronger, causing the natural wavelength of the air to match the size of the hill (Fig 14.14c). Large-amplitude *lee waves* or *mountain waves* are formed by such a natural resonance, with the possibility of rotor circulations near the ground under the wave crests. For this case, the air at the surface stagnates at periodic intervals downwind of the hill, and reverse flow can occur at the surface under the rotors. If sufficient moisture is present, *standing lenticular clouds* can form along the crests of the waves, and *rotor clouds* can form in the updraft portion of the rotor circulations.
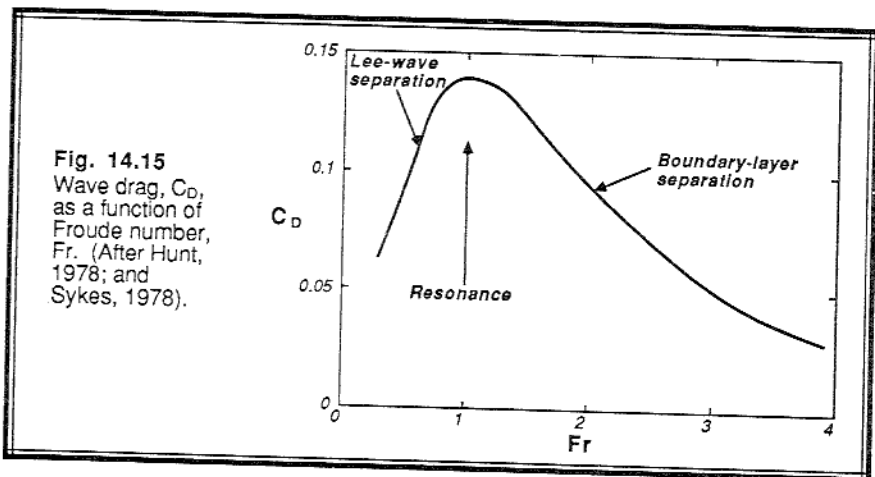
Fig. 14.15
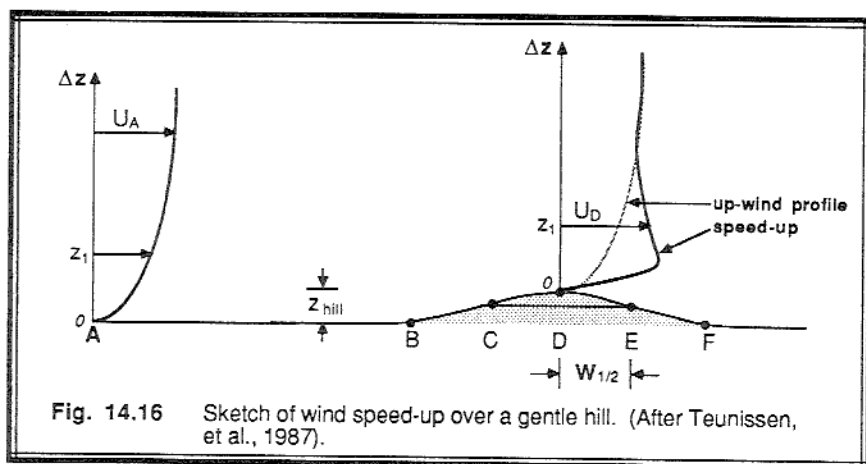Wave drag, C_D, as a function of Froude number, Fr. (After Hunt, 1978; and Sykes, 1978).

For even stronger winds and weaker stability (Fr $\cong$ 1.7) the natural wavelength is longer than the hill dimensions. This causes *boundary layer separation* at the lee of the hill, and creates a *cavity* with reverse surface wind direction immediately behind the hill (Fig 14.14d). Wave drag associated with flow over a hill is a maximum for the resonance state, and is less for lee-wave and boundary-layer separation (Fig 14.15).

Neutral Stratification. For strong winds and neutral stability, the Froude number approaches infinity, and is not an appropriate measure of flow dynamics. Flow of a neutral boundary layer over an isolated hill is sketched in Fig 14.14e. Streamlines are disturbed upwind and above the hill out to a distance of about three times the size of the hill. Beyond this *region of influence*, the flow does not "feel" the presence of the hill. Near the top of the hill the streamlines are packed closer together, causing a *speed-up* of the wind.

Immediately downwind of the hill in strong wind situations, there is often found a *cavity* (sometimes called a *wind shadow*) associated with boundary layer separation (Tampieri, 1987). This is the start of a turbulent *wake* behind the hill. The height of the wake is initially on the same order as the size of the hill, but it grows in size and decreases in turbulence intensity further downwind of the hill. Eventually, in the absence of other turbulence generating mechanisms, the turbulence decays completely far downwind of the hill, and the flow returns to its undisturbed state. Similar flow patterns are found near buildings (Hanna, et al., 1982). For weaker winds and smooth gentle hills, the cavity and turbulent wake sometimes do not form (Taylor, et al., 1987).

The speed-up at the crest of the hill is sketched in Fig 14.16. The fractional speed-up ratio, $\Delta\overline{M}_{hill}$ is defined as:

$$\Delta\overline{M}_{hill} = \frac{\overline{M}_x(\Delta z) - \overline{M}_A(\Delta z)}{\overline{M}_A(\Delta z)} \tag{14.2.3c}$$

Fig. 14.16   Sketch of wind speed-up over a gentle hill. (After Teunissen, et al., 1987).

where Δz is the height above the local terrain, and subscript A denotes a point upwind of the hill where the flow is undisturbed. For gentle 2-D ridges, speed-up values of about

$\Delta \overline{M}_{hill} \cong 2 \; z_{hill}/W_{1/2}$ are expected, while for isolated 3-D hills the speed-up is less,

$\Delta \overline{M}_{hill} \cong 1.6 \; z_{hill}/W_{1/2}$ (Taylor & Teunissen, 1987; Taylor & Lee, 1984; Hunt, 1980). The half width of the hill, $W_{1/2}$, is defined as the horizontal upstream distance from the crest to the point where the elevation has decreased to half its maximum. For typical gentle hills ($z_{hill} = 100$ m, $W_{1/2} = 250$ m) the speed-up of the wind just above the crest of the hill can be 60% or more, which is important for siting wind-turbine generators.

Fig 14.17 shows the wind speed profiles at various locations on the hill (Teunissen, et al., 1987). Well upwind at point A, out of the region of influence, the wind is logarithmic with height as expected for neutral stratification. Closer to the hill, at point B, some blocking is experienced and the low-altitude winds are slower. By point C, the winds above 2 m have accelerated beyond the undisturbed upstream values, and even become faster than ambient winds aloft at point D at the crest of the hill. To the lee of the hill, the low-altitude winds rapidly decrease, and can become slower than the undisturbed upstream values, or can reverse direction as discussed earlier.
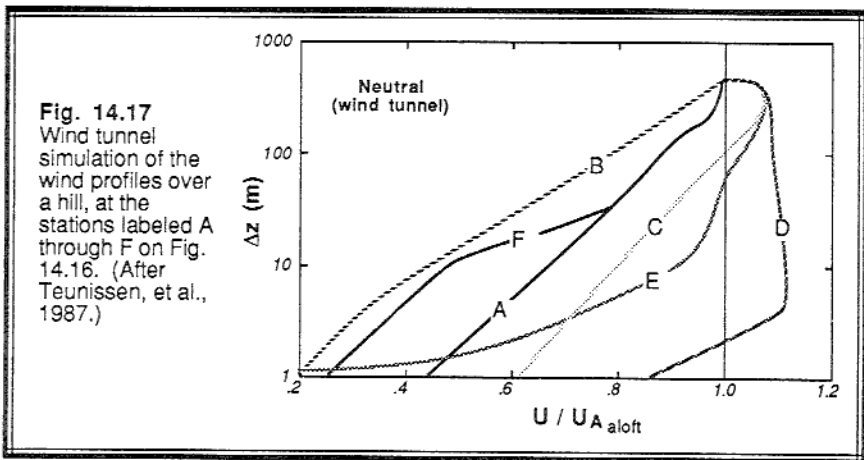
Fig. 14.17 Wind tunnel simulation of the wind profiles over a hill, at the stations labeled A through F on Fig. 14.16. (After Teunissen, et al., 1987.)

The height of the maximum speed-up can be estimated using the roughness length and mountain half width:

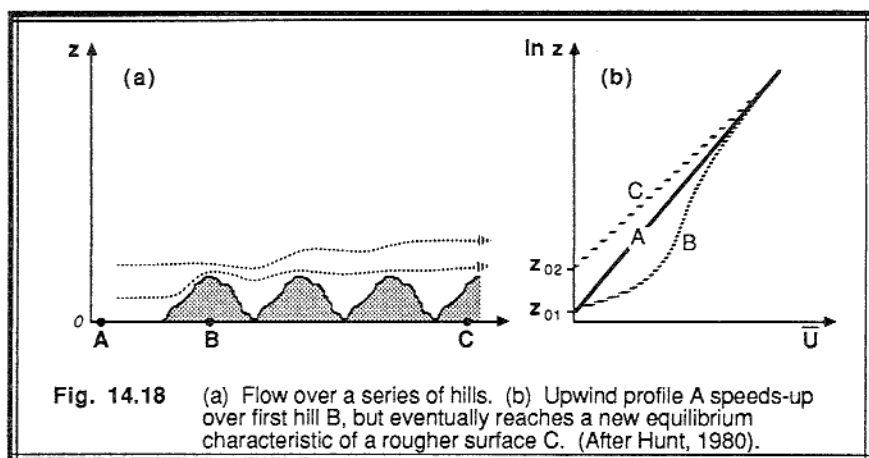$$\Delta z_{max} \cong z_o \; e^{(2 k^2 W_{1/2})^b} \qquad (14.2.3d)$$

Below this height is an *inner layer* where friction with the ground reduces the wind speed. Above this height in an *outer layer*, the flow can be well described by inviscid *potential flow theory*.

Suggestions for the value of b range from 0.5 to 1.0 (Taylor and Teunissen, 1987; Jackson and Hunt, 1975; and Jensen, et al., 1984; Zeman and Jensen, 1987), but it appears that 0.5 gives the best agreement with observations. For many of the gentle hills reviewed by Taylor, et al. (1987), the height above the hill crest where the maximum speed-up is found ranges between 2.5 and 5 m. The inner layer for the hill of Fig 14.17, for example, is about 3.5 m thick at point D. Thus, we see that the inner layer is quite shallow.

In the outer layer, some of the changes to the turbulence field appear to be described by *rapid distortion theory* (Taylor, et al., 1987). This theory assumes that existing eddies are distorted by the flow over the hill, and that the turbulence is modified by compression and stretching of the existing vortex elements (Britter, et al., 1981; Panofsky, et al., 1982). The theory further assumes that the distortion is rapid enough that turbulence generation by the mechanical production terms is not increased. Rapid distortion theory predicts that $\overline{w'^2}$ will increase over a 2-D ridge, but $\overline{u'^2}$ will decrease in the outer layer. The vortex stretching also enhances the higher frequencies of turbulence, and reduces the lower frequencies. Observations, however, indicate that both $\overline{w'^2}$ and $\overline{u'^2}$ are reduced in the outer layer.

In the inner layer, where wind shears are enhanced and turbulence is in local equilibrium with the surface, most turbulence statistics (including stress) are larger than their upstream values (Taylor, et al., 1987). Zeman and Jensen (1987) have suggested a third layer in between the inner and outer layers. This layer occurs at roughly the height of maximum speed-up, and is characterized by a minimum in turbulent stresses as a consequence of the curvature of the mean flow streamlines. Analogous curvature effects are believed to be related in increases in turbulence statistics upstream of the hill crest.

A series of hills can modify the flow to yield a new log-wind profile that has an aerodynamic roughness length characteristic of rough terrain (Fig 14.18). Over the first

Fig. 14.18   (a) Flow over a series of hills. (b) Upwind profile A speeds-up over first hill B, but eventually reaches a new equilibrium characteristic of a rougher surface C. (After Hunt, 1980).

hill, the wind profile experiences the speed-up already discussed. Over succeeding hills, the superposition of the effects from the individual hills accumulate to generate a wind profile that is slower at low levels, characteristic of a larger roughness length (Hunt, 1980).

Mixed Layer Capped by an Inversion. Some interesting phenomena can occur when a mixed layer approaches a 2-D ridge (Fig 14.19), because the capping inversion tends to constrain the flow response to occur within the mixed layer. Define a modified Froude number, Fr*, by:

$$\text{Fr*} = \frac{\overline{M}}{N_{BV} \cdot (z_i - z_{hill})} \tag{14.2.3e}$$

For $z_i > z_{hill}$, two different types of flow can occur depending on the wind speed (Hunt, 1980; Carruthers and Choularton 1982). For relatively slow wind speeds (Fr* $\ll$ 1), acceleration over the ridge crest can locally draw down the inversion via a *Bernoulli* mechanism (Fig 14.19a). To the lee of the ridge light winds are found in the region of boundary-layer separation.

For faster winds (Fr* $\cong$ 1) with a strong capping inversion, the mixed layer accelerates down the lee side of the mountain in a very shallow high-velocity flow (Fig 14.19b) that is sometimes called a *downslope windstorm* in the Boulder, Colorado area, or *bora* in Yugoslavia. Wind gusts greater than 50 m/s have been measured in Boulder during one of these severe downslope winds, with substantial damage to houses and trees and aircraft reports of severe to extreme turbulence (Lilly, 1978). The bora can last 4 to 6 days (Smith, 1987). Downwind of the ridge there can be a *hydraulic jump*, where the boundary layer rapidly decelerates and the depth increases. The hydraulic jump can be visualized as a wave or bore that is trying to propagate upstream, in a flow that is fast enough to counteract any propagation towards the mountain. Two-layer models capture most of the important physics of this phenomenon, while three-layers offer more accuracy (Smith and Sun, 1987).

If $z_i \gg z_{hill}$, then the mixed layer tends to evolve as if the hill were not present. This is particularly true for light winds and strong convection. For a high isolated 3-D mountain and a shallow boundary layer ($z_i < z_{hill}$), the air is constrained to flow around the mountain (Fig 14.19c). This can cause a street of *von Karman vortices* (Brighton, 1978) to form downwind of the mountain (Fig 14.19d).

14.2.4 Flow Over Other Complex Terrain

Many other phenomena can occur for various valley and pass geometries (Egan, 1975). Boundary layer winds can be funneled through mountain passes, generating strong pass winds. Ambient flow crossing narrow valleys can generate both along-valley flow and cross-valley circulations within the valley (Erasmus, 1986a and b). Differential
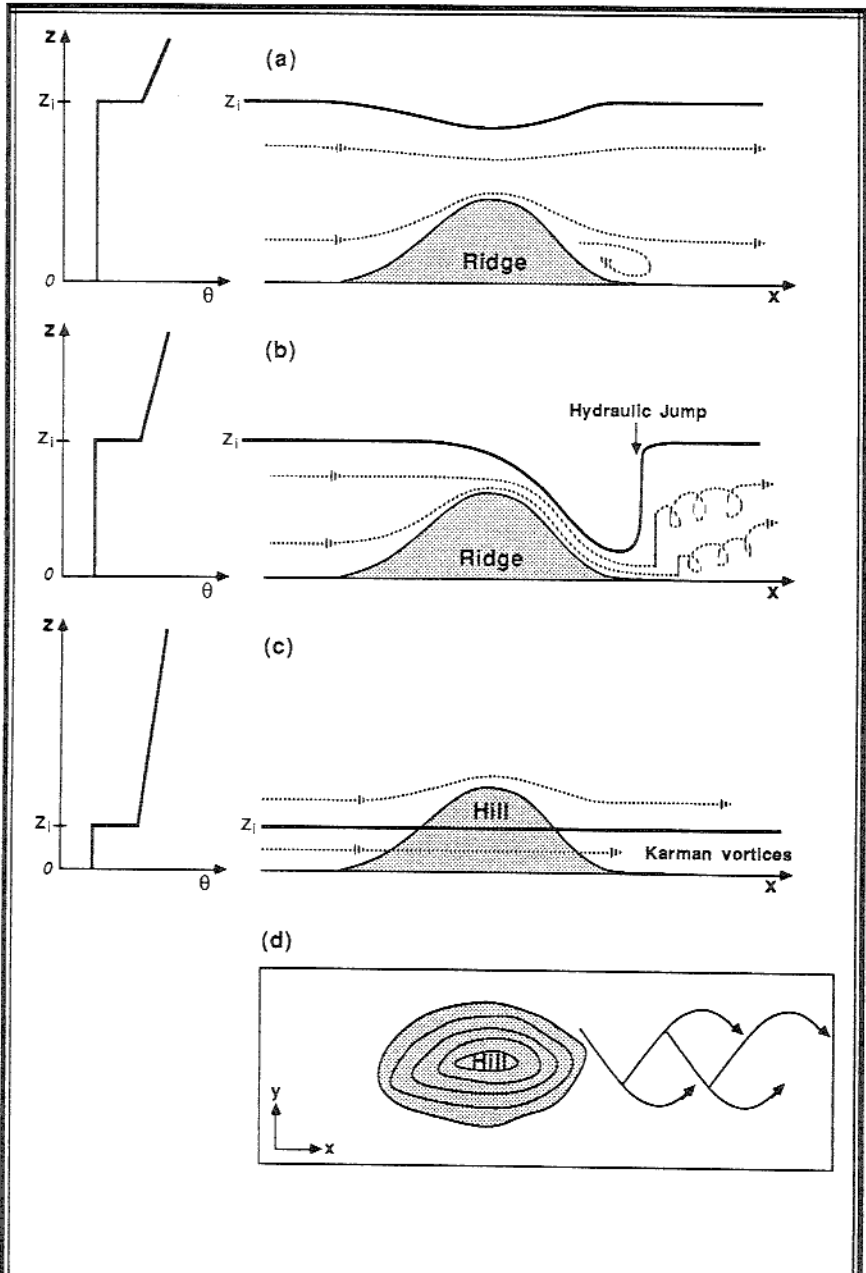
Fig. 14.19   (a) Bernoulli effect as flow accelerates over a 2-D ridge; (b) hydraulic jump downwind of a 2-D ridge for greater ambient wind speed; (c) flow around the sides of an isolated hill; and (d) Karman vortex street downwind of the hill from (c). (After Hunt, 1980.)

solar heating of one valley wall compared to the other can modify the turbulence intensity and stress (Carlson and Foster, 1986). Pollutant dispersion in complex terrain is difficult to model, and additional research is needed in this area (Egan and Schiermeier, 1986).

In large cities, tall buildings act like steep valley walls along **urban canyons** formed by the streets (Oke, 1978). As might be expected, the criss-crossing urban canyons for a very complex urban terrain system, with air being trapped in some canyons and air in others being ducted like wind-tunnels (Hosker, 1987). Not only is there differential absorption on the various canyon walls (buildings) depending on the sun position, but there can be significant multiple reflections off of the windows and emission of heat from traffic in the street and from buildings (Johnson and Watson, 1984; Steyn and Lyons, 1985). The generation of urban boundary layers is reviewed after the example below.

14.2.5 Example

Problem. Air is flowing from a corn field to a short-cut grass pasture. How far downwind from the edge of the corn field should a 10 m mast be erected so as to not "feel" the influence of the corn field (i.e., what minimum fetch within the pasture is required). Assume statically neutral conditions, and no change of surface heat flux.

Solution. First, we can estimate the roughness of the two fields using Fig 9.6: for corn, $z_{o1} \cong 0.06$; for cut grass, $z_{o2} \cong 0.006$. Using (14.2.1b) we can solve for the a_{IBL} parameter:

$$a_{IBL} = 0.75 + 0.03 \ln\left(\frac{0.006}{0.06}\right) = 0.681$$

Next, we can solve (14.2.1a) for the required fetch, knowing that δ must be at least 10 m:

$$x = z_{o1} \cdot \left(\frac{1}{a_{IBL}} \frac{\delta}{z_{o1}}\right)^{1/b_{IBL}} = 0.06 \cdot \left(\frac{1}{0.681} \frac{10}{0.06}\right)^{1/0.8} = 58 \text{ m}$$

Discussion. The mast must be located no less that 58 m from the corn field. If we anticipate a range of stabilities during our measurement, it would be best to locate the mast even further away. Note that the equation for IBL depth is not a function of wind speed, because it is assumed that turbulence is more intense and the IBL grows faster in a surface layer with greater shear.
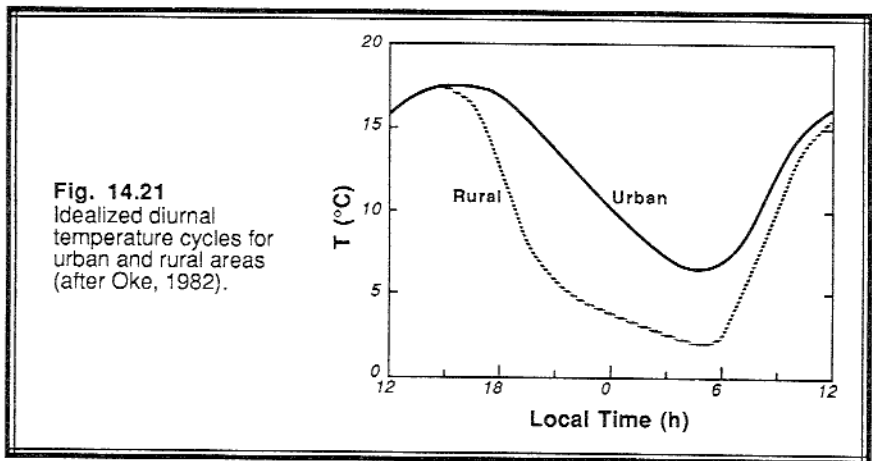
14.3 Urban Heat Island and the Urban Plume

Most cities are anthropogenic sources of heat and pollution. In addition, the downtown areas are covered by a large percentage of asphalt and concrete, which are usually dry, water-proof surfaces with albedoes and heat capacities that convert and store incoming radiation as sensible heat better than the surrounding countryside (recall Fig
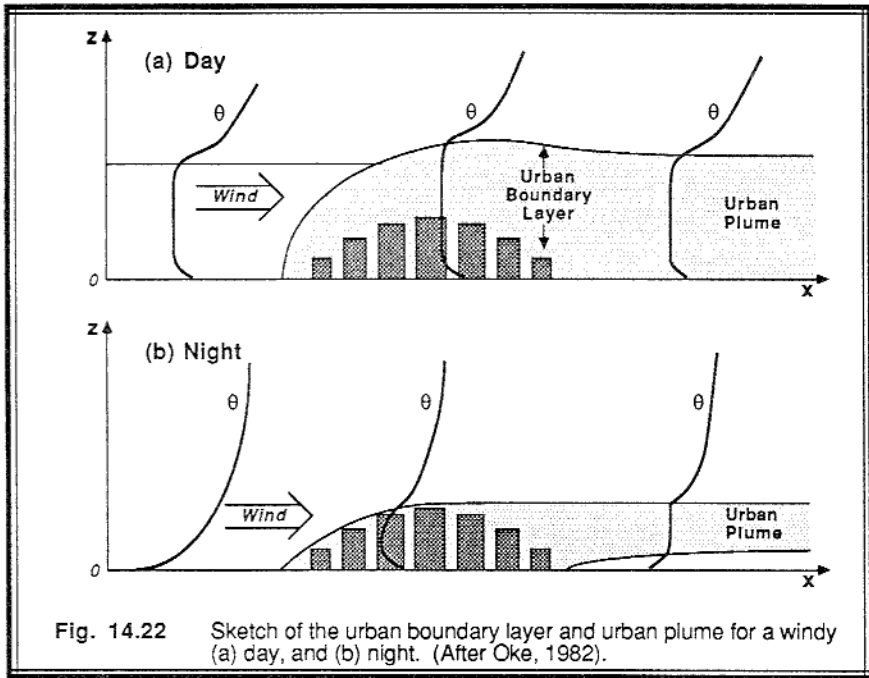
7.12). Thus, surface-layer air in cities is generally warmer than that of their surroundings (Oke, 1982, 1987; Goldreich, 1985; Bornstein, 1987). When isotherms are plotted on a surface weather map, the pattern looks like the topographic contours of an island (Fig 14.20), whence the term *heat island*.

Fig. 14.20
Idealized isotherm
heat-island pattern
over an urban area
(shaded). (After
Oke, 1982).
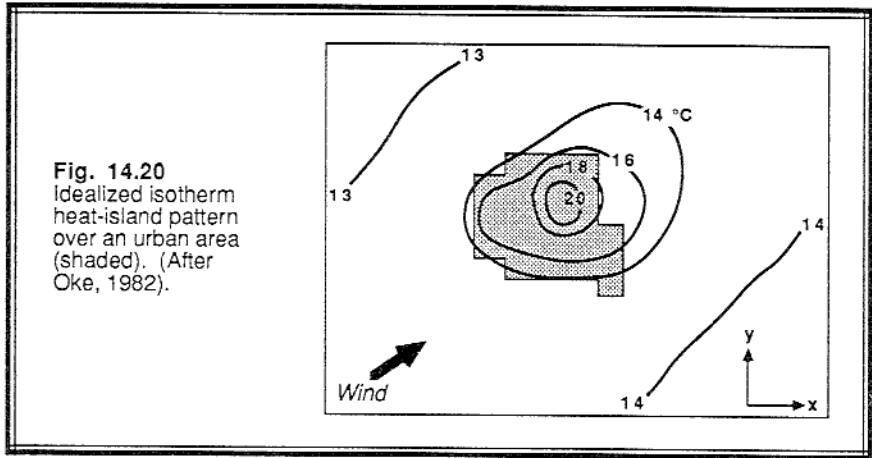
The greatest temperature differences between urban and rural areas are usually observed during the night (Fig 14.21). In many cases, heat from the city is sufficient to maintain a shallow convective mixed layer at night, even while a substantial stable boundary layer has developed over the surrounding countryside (Fig 14.22). Cities with a population of about 1000 have been observed to have maximum temperature excesses (compared to the surrounding rural area) of 2 to 3 °C, while cities of a million or more inhabitants have been known to generate excesses of 8 to 12°C (Oke, 1982; Katsoulis and Theoharatos, 1985).

Fig. 14.21
Idealized diurnal
temperature cycles for
urban and rural areas
(after Oke, 1982).

Fig. 14.22   Sketch of the urban boundary layer and urban plume for a windy (a) day, and (b) night. (After Oke, 1982).

Synoptic and topographic forcings influence the development of the urban boundary layer. The temperature excesses at any given time are modulated by cloudiness, precipitation, and mean ambient wind speed (Ackerman, 1985; McKee, et al., 1987). Local topography such as mountains, lakes and rivers also have a large impact. In Chicago, for example, the greatest temperature excess is often observed in early evening during the late summer.

Enhanced urban turbulence at night can create counter-rotating vortices on opposite sides of the city (Draxler, 1986). Balling and Cerveny (1987) noted an increase in wind speed over the city at night, which they suggested was due to local urban horizontal temperature gradients and enhanced vertical mixing with the faster flow aloft.

During the daytime, heat from the urban area can enhance the mixing already present in the ML, and create an urban internal boundary layer. Hildebrand and Ackerman (1984) and Clarke, et al. (1987) reported enhanced turbulent heat flux, vertical velocity variance, and entrainment rates over urban areas. The ML can sometimes be deeper over urban areas than rural ones because of greater low-level convergence, resulting in more cloud condensation nuclei, more thunderstorms and enhanced precipitation immediately downwind of the city (Changnon, 1981). The presence of large buildings increases surface drag and wake turbulence, and decreases the mean wind speed.

In the presence of a mean wind, excesses of temperature and pollutants, and deficits of humidity are carried downwind in an ***urban plume*** (Oke, 1982; Hanna, et al., 1987).

These plumes are as wide as the city, and can be transported hundreds of kilometers downstream (Fig 14.21). In the absence of wind, closed circulations analogous to the sea-breeze can form over the city (Fig 14.23).

Fig. 14.23   Local circulations induced over a warm city during calm ambient flow.
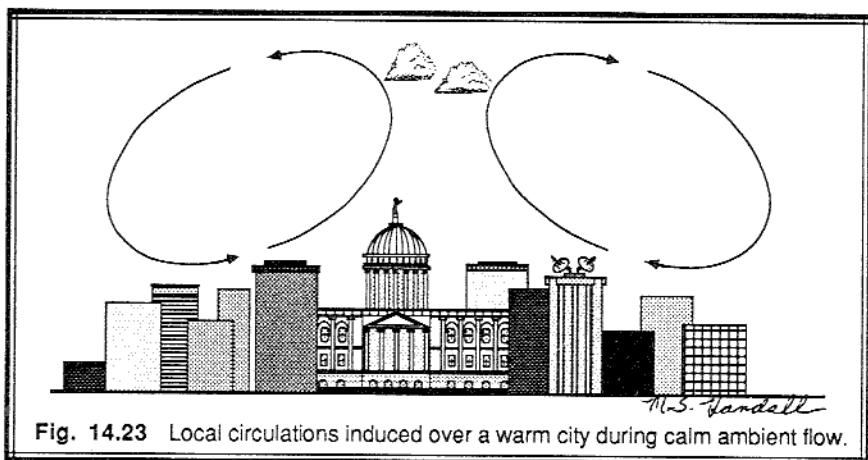
The portion of boundary layer between the roof tops and the ground is known as the *urban canopy layer*, by analogy with plant canopies (Oke, 1987). Within this region we find the urban canyons, ducting and trapping of air flow, and multiple reflections of radiation previously discussed. Above that is the *turbulent wake layer*, where the wakes and IBLs from the individual buildings and surface patterns can still be discerned (Fig 14.24). Still higher is the surface layer, where the momentum and heat budgets feel the average effect of the urban area, but where individual wakes are not important. Finally, the urban mixed layer extends to the top of the urban boundary layer, which itself might be an internal boundary layer within the larger-scale flow.

Fig. 14.24   Layers within the urban boundary layer. (After Oke, 1987).
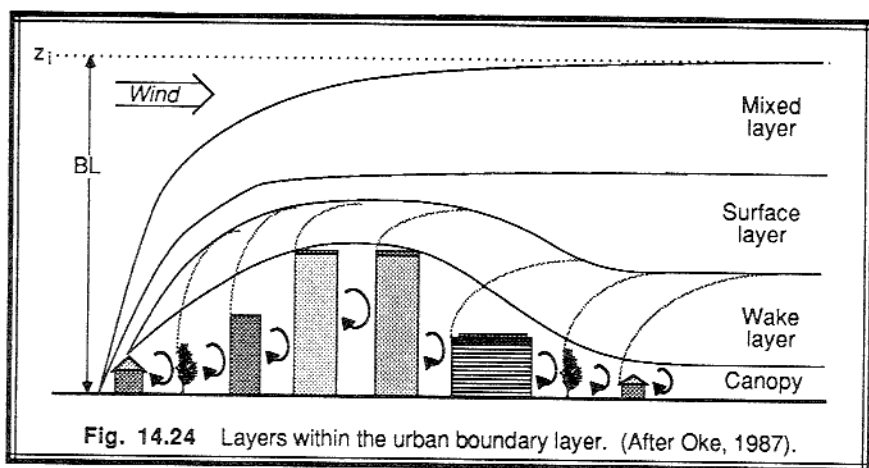
14.4 References

Ackerman, B., 1985: Temporal march of the Chicago heat island. *J. Clim. Appl. Meteor.*, **24**, 547-554.

Arritt, R.W., 1987: Effect of water surface temperature on lake breezes and thermal internal boundary layers. *Bound.-Layer Meteor.*, **40**, 101-125.

Balling, R.C., Jr. and R.S. Cerveny, 1987: Long-term associations between wind speeds and the urban heat island of Phoenix, Arizona. *J. Clim. Appl. Meteor.*, **26**, 712-716.

Banta, R.M., 1985: Late-morning jump in TKE in the mixed layer over a mountain basin. *J. Atmos. Sci.*, **42**, 407-411.

Beljaars, A.C.M., 1987: On the memory of wind standard deviation for upstream roughness. *Bound.-Layer Meteor.*, **38**, 95-102.

Beljaars, A.C.M., J.L. Walmsley, P.A. Taylor, 1987: A mixed spectral finite difference model for neutrally stratified boundary layer flow over roughness changes and topography. *Bound. Layer Meteor.*, **38**, 273-303.

Bornstein, R.D., 1987: Mean diurnal circulation and thermodynamic evolution of urban boundary layers. *Modeling the Urban Boundary Layer*. Amer. Meteor. Soc., Boston. 53-93.

Briere, S., 1987: Energetics of daytime sea breeze circulation as determined from a two-dimensional, third-order turbulence closure model. *J. Atmos. Sci.*, **44**, 1455-1474.

Brighton, P.W.M., 1978: Strongly stratified flow past three-dimensional obstacles. *Quart. J. Roy. Meteor. Soc.*, **104**, 289-308.

Britter, R.E., J.C.R. Hunt and K.J. Richards, 1981: Airflow over a two-dimensional hill: studies of velocity speed-up, roughness effects and turbulence. *Quart. J. Roy. Meteor. Soc.*, **107**, 91-110.

Brutsaert, W. and W.P. Kustas, 1987: Surface water vapor and momentum fluxes under unstable conditions from a rugged complex area. *J. Atmos. Sci.*, **44**, 421-431.

Carlson, J.D. and M.R. Foster, 1986: Numerical study of some unstably stratified boundary-layer flows over a valley at moderate Richardson number. *J. Clim. Appl. Meteor.*, **25**, 203-213.

Carruthers, D.J. and T.W. Choularton, 1982: Airflow over hills of moderate slope. *Quart. J. Roy. Meteor. Soc.*, **108**, 603-624.

Changnon, S.A., Jr. (Ed.), 1981: *METROMEX: A Review and Summary*. Meteor. Monographs, 18, No. 40. Amer. Meteor. Soc., Boston. 181pp.

Clarke, J.F., J.K.S. Ching, J.M. Goodwitch, and F.S. Binkowski, 1987: Surface layer turbulence in an urban area. *Modeling the Urban Boundary Layer*. Amer. Meteor. Soc., Boston. 161-199.

Claussen, M., 1987: The flow in a turbulent boundary layer upstream of a change in surface roughness. *Bound.-Layer Meteor.*, **40**, 31-86.

Draxler, R.R., 1986: Simulated and observed influence of the nocturnal urban heat island on the local wind field. *J. Clim. Appl. Meteor.*, **25**, 1125-1133.

Egan, B.A. and F.A. Schiermeier, 1986: Dispersion in complex terrain: a summary of the AMS workshop held in Keystone, Colorado, 17-20 May 1983. *Bull. Amer. Meteor. Soc.*, **67**, 1240-1247.

Erasmus, D.A., 1986: A model for objective simulation of boundary-layer winds in an area of complex terrain. *J. Clim. Appl. Meteor.*, **25**, 1832-1841.

Erasmus, D.A., 1986: A comparison of simulated and observed boundary-layer winds in an area of complex terrain. *J. Clim. Appl. Meteor.*, **25**, 1842-1852.

Fitzjarrald, D.R., 1984: Katabatic wind in opposing flow. *J. Atmos. Sci.*, **41**, 1143-1158.

Fitzjarrald, D.R., 1986: Slope winds in Veracruz. *J. Clim. Appl. Meteor.*, **25**, 133-144.

Garratt, J.R., 1983: Surface influence upon vertical profiles in the nocturnal boundary layer. *Bound.-Layer Meteor.*, **26**, 69-80.

Garratt, J.R., 1987: The stably stratified internal boundary layer for steady and diurnally varying offshore flow. *Bound.-Layer Meteor.*, **38**, 369-394.

Gash, J.H.C., 1986: A note on estimating the effect of a limited fetch on micrometeorological evaporation measurements. *Bound.-Layer Meteor.*, **35**, 409-413.

Geiger, R., 1965: *The Climate Near the Ground, Revised Edition.* Harvard Univ. Press, Cambridge. 611 pp.

Goldreich, Y., 1985: The structure of the ground-level heat island in a central business district. *J. Clim. Appl. Meteor.*, **24**, 1237-1244.

Hanna, S.R., 1987: An empirical formula for the height of the coastal internal boundary layer. *Bound.-Layer Meteor.*, **40**, 205-207.

Hanna, S.R., G.A. Briggs, and R.P. Hosker, Jr., 1982: *Handbook on Atmospheric Diffusion.* Tech. Information Center, U.S. Dept. of Energy. DOE/TIC-11223. 102pp.

Hanna, S.R., J.V. Ramsdell, and H.E. Cramer, 1987: Urban Gaussian diffusion parameters. *Modeling the Urban Boundary Layer.* Amer. Meteor. Soc., Boston. 337-379.

Haugen, D.A.(Ed.), 1975: *Lectures on Air Pollution and Environmental Impact Analysis.* Amer. Meteor. Soc., Boston. 296pp.

Helmis, C.G., D.N. Asimakopoulos, D.g. Deligiorgi, and D.P. Lalas, 1987: Observations of sea-breeze fronts near the shoreline. *Bound.-Layer Meteor.*, **38**, 395-410.

Hildebrand, P.H., and B. Ackerman, 1984: Urban effects on the convective boundary layer. *J. Atmos. Sci.*, **41**, 76-91.

Hosker, R.P., Jr., 1987: Effects of buildings on local dispersion. *Modeling the Urban Boundary Layer.* Amer. Meteor. Soc., Boston. 95-160.

Hsu, S.A., 1986: A note on estimating the height of the convective internal boundary layer near shore. *Bound.-Layer Meteor.*, **35**, 311-316.

Hunt, J.C.R., 1980: Wind over hills. *Workshop on the Planetary Boundary Layer.* J.C. Wyngaard (Ed.), Amer. Meteor. Soc., Boston. 107-144.

Jackson, P.S. and J.C.R. Hunt, 1975: Turbulent wind flow over a low hill. *Quart. J. Roy. Meteor. Soc.*, **101**, 929-956.

Jensen, N.O., E.L. Petersen, and I. Troen, 1984: *Extrapolation of Mean Wind Statistics with Special Regard to Wind Energy Applications.* Report WCP-86, WMO, Geneva. 85pp.

Johnson, G.T. and I.D. Watson, 1984: The determination of view-factors in urban canyons. *J. Clim. Appl. Meteor.*, **23**, 329-335.

Johnson, G.T. and I.D. Watson, 1985: Reply. *J. Clim. Appl. Meteor.*, **24**, 386.

Katsoulis, B.D. and G.A. Theoharatos, 1985: Indications of the urban heat island in Athens, Greece. *J. Clim. Appl. Meteor.*, **24**, 1296-1302.

Kitada, T., K. Igaraschi and M. Owada, 1986: Numerical analysis of air pollution in a combined field of land/sea breeze and mountain/valley wind. *J. Clim. Appl. Meteor.*, **25**, 767-784.

Lilly, D.K., 1978: A severe downslope windstorm and aircraft turbulence event induced by a mountain wave. *J. Atmos. Sci.*, **35**, 59-77.

Lyons, W.A., 1975: Turbulent diffusion and pollutant transport in shoreline environments. *Lectures on Air Pollution and Environmental Impact Analysis*, D.A. Haugen (Ed.), Am. Meteor. Soc. 136-208.

Martin, C.L. and R.A. Pielke, 1983: The adequacy of the hydrostatic assumption in sea breeze modeling over flat terrain. *J. Atmos. Sci.*, **40**, 1472-1481.

McKee, T.B., D.C. Bader, and K. Hanson, 1987: Synoptic influence on urban circulation. *Modeling the Urban Boundary Layer.* Amer. Meteor. Soc., Boston. 201-214.

McNider, R.T. and R.A. Pielke, 1984: Numerical simulation of slope and mountain flows. *J. Clim. Appl. Meteor.*, **23**, 1441-1453.

Mitsuta, Y., N. Monji, and D.H. Lenschow, 1986: Comparisons of aircraft and tower measurements around Tarama Island during the AMTEX '75. *J. Clim. Appl. Meteor.*, **25**, 1946-1955.

Neff, W.D. and C.W. King, 1987: Observations of complex-terrain flows using acoustic sounders: experiments, topography, and winds. *Bound.-Layer Meteor.*, **40**, 363-392.

Noonan, J.A. and R.K. Smith, 1986: Sea-breeze circulations over Cape York Peninsula and the generation of Gulf of Carpentaria cloud line disturbances. *J. Atmos. Sci.*, **43**, 1679-1693.

Ogawa, Y., T. Ohara, S. Wakamatsu, P.G. Diosey, and I. Uno, 1986: Observations of lake breeze penetration and subsequent development of the thermal internal boundary layer for the Nonticoke II shoreline diffusion experiment. *Bound.-Layer Meteor.*, **35**, 207-230.

Oke, T.R., 1978: *Boundary Layer Climates.* Halsted Press, New York. 372pp.

Oke, T.R., 1982: The energetic basis of the urban heat island. *Quart. J. Roy. Meteor. Soc.*, **108**, 1-24.

Oke, T.R., 1987: The surface energy budgets of urban areas. *Modeling the Urban Boundary Layer.* Amer. Meteor. Soc., Boston. 1-52.

Panofsky, H.A., D. Larko, R. Lipschutz, G. Stone, E.F. Bradley, A.J. Bowen, J.Højstrup, 1982: Spectra of velocity components over complex terrain. *Quart. J. Roy. Meteor. Soc.*, **108**, 215-230.

Pearson, R.A., G. Carboni and G. Brusasca, 1983: The sea breeze with mean flow. *Quart. J. Roy. Meteor. Soc.*, **109**, 809-830.

Rao, K.S., J.C. Wyngaard and O.R. Coté, 1974: The structure of the two-dimensional internal boundary layer over a sudden change of surface roughness. *J. Atmos. Sci.*, **31**, 738-746.

Rotunno, R., 1983: On the linear theory of the land and sea breeze. *J. Atmos. Sci.*, **40**, 1999-2009.

Simpson, J.E., D.A. Mansfield, J.R. Milford, 1977: Inland penetration of sea-breeze fronts. *Quart. J. Roy. Meteor. Soc.*, **103**, 47-76.

Smedman-Högström, A.-S., and U. Högström, 1978: A practical method for determining wind frequency distributions for the lowest 200 m from routine meteorological data. *J. Appl. Meteor.*, **17**, 942-954.

Smith, R.B., 1987: Aerial observations of the Yugoslavian Bora. *J. Atmos. Sci.*, **44**, 269-297.

Smith, R.B. and J. Sun, 1987: Generalized hydraulic solutions pertaining to severe downslope winds. *J. Atmos. Sci.*, **44**, 2934-2939.

Steyn, D.G. and T.J. Lyons, 1985: Comments on "The determination of view-factors in urban canyons". *J. Clim. Appl. Meteor.*, **24**, 383-385.

Sykes, R.I. 1978: Stratification effects in boundary layer flow over hills. *Proc. Roy. Soc.* A.

Tampieri, F., 1987: Separation features of boundary-layer flow over valleys. *Bound.-Layer Meteor.*, **40**, 295-308.

Taylor, P.A., P.J. Mason and E.F. Bradley, 1987: Boundary-layer flow over low hills (A review). *Bound.-Layer Meteor.*, **39**, 107-132.

Taylor, P.A. and H.W. Teunissen, 1987: The Askervein Project: overview and background data. *Bound.-Layer Meteor.*, **39**, 15-39.

Teunissen, H.W., M.E. Shokr, A.J.Bowen, C.J. Wood, and D.W.R. Green, 1987: The Askervein Hill Project: wind tunnel simulations at three length scales. *Bound.-Layer Meteor.*, **40**, 1-29.

Venkatram, A., 1977: A model for internal boundary layer development. *Bound.-Layer Meteor.*, **11**, 419-437.

Wakimoto, R.M. and J.L. McElroy, 1986: Lidar observation of elevated pollution layers over Los Angeles. *J. Clim. Appl. Meteor.*, **25**, 1583-1599.

Whiteman, C.D., 1982: Breakup of temperature inversions in deep mountain valleys: part 1. observations. *J. Appl. Meteor.*, **21**, 270-289.

Wood, D.H., 1978: Calculation of the neutral wind profile following a large step change in surface roughness. *Quart. J. Roy. Meteor. Soc.*, **104**, 383-392.

Zeman, O. and N.O. Jensen, 1987: Modification of turbulence characteristics in flow over hills. *Quart. J. Roy. Meteor. Soc.*, **113**, 55-80.

14.5 Exercises

1) Define each of the layers below:
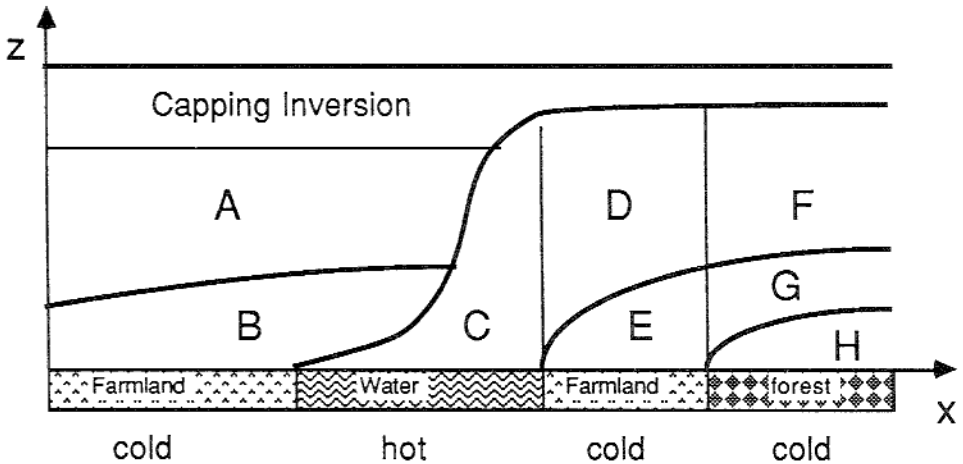
2) Given the surface-layer wind profile at right, explain all the possible reasons why the line is not straight when plotted on a semi-log graph.
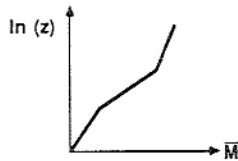
3) Given the wind profile at right, determine whether the boundary layer is flowing from smooth to rough or rough to smooth, and estimate the distance upwind at which the change in roughness occurred. Assume neutral static stability and zero displacement height.
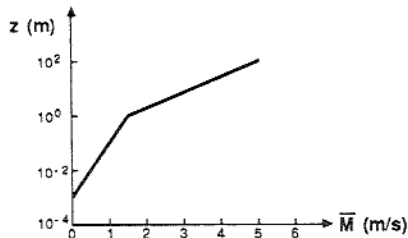
4) Assume a slab mixed layer of initial depth $z_i = 100$ m, with an initial potential temperature of 280 K. This air is advecting from land to warmer water (water surface effective potential temperature is 290 K) with a mean wind speed of 5 m/s. Over land, there is no flux into the bottom of the mixed layer, and no entrainment into the top. Over water, the flux at the bottom can be approximated with a bulk transfer relationship (use $C_D = 2 \times 10^{-3}$). The flux ratio method can be used to model the entrainment across the top. Neglect subsidence, and assume for simplicity that the strength of the capping inversion is always 2 K.

a) Calculate and plot the IBL depth and slab potential temperature as a function of downwind distance, x.

b) How does the thickness and temperature at x = 1 km downwind of the shoreline

vary with wind speed.

5) Suppose that the air flowing over two hills is statically stable. The stability is such that the Froude number for the first hill is Fr = 0.5.

a) Sketch the flow over the first hill.

b) If the second hill is half the width of the first hill, what is its Froude number, and sketch the flow over it, assuming the same stability and wind speed as for the first hill.

6) What is the Froude number, and how is it used?

7) What is an anabatic cumulus cloud?

8) Given a wide valley with ridges on both sides, describe the dispersion of smoke over a full diurnal cycle from two stacks:

a) One very short stack at the side of the valley floor at the base of the ridge.

b) A tall stack (100 m) at the same location as in part (a).

9) If a fully enclosed basin fills with cold air during the night, describe the flow across the top of the cold pool of air in the morning. State all your assumptions.

10) If a sea breeze is caused by warm air rising over land surface during the day, then what causes the low-level inflow from sea to land?

11) Why is the equation for depth of the internal boundary layer (14.2.1a) not a function of wind speed?

12) Plot the depth of the IBL as a function of distance downwind of a change in roughness, given $z_{o1} = 10^{-3}$ m and $z_{o2} = 10^{-2}$ m. State your assumptions.

13) Suppose air is flowing from warm land over a cooler lake during the Spring.

a) If the wind speed is 7 m/s and the lake is 15°C cooler than the land surface (290 K), then plot the depth of the stable TIBL as a function of distance from the shore.

b) If the same situation occurs in the Fall, except that the land and lake temperatures are reversed, plot the depth of the convective TIBL as a function of distance downwind from the shore.

c) Compare the plots from (a) and (b), and explain why they differ.

14) Assume the mean wind speed is 5 m/s, the hill width is 200 m, and the vertical potential temperature gradient is 0.02 K/m.

a) Calculate the Froude number.

b) Above what height does flow separate and flow over the hill. Assume the hill is 100 m high.

c) Calculate the amount of speed-up at the crest of the hill, and the height above the hill at which this speed-up is found. State your assumptions.

d) What other factors besides speed-up might be important for determining whether a site could be used for wind turbine power generation?

17) Assuming an exponential change of temperature with height in the SBL (see Chapter 12) and a hill of width and height 500 m, calculate and plot the Froude number as a function of height. Sketch a possible flow field for this situation.

18) Given an ambient wind speed of 15 m/s and a mountain height of 1000 m, plot a curve of lapse rate vs. depth of the mixed layer that delineates the threshold for the onset of severe downslope windstorms.

19) Describe the nature of the urban boundary layer for your own town.